

MODELING STRUCTURAL AND MAGNETIC PHASE TRANSITIONS IN IRON–NICKEL NANOPARTICLES

K. KADAU^a, M. GRUNER^b, P. ENTEL^{b,*} and M. KRETH^b

^a*Los Alamos National Laboratory, T-11, MS B262, Los Alamos, NM 87545, USA;*

^b*Institute of Physics, Gerhard-Mercator-University, 47048 Duisburg, Germany*

Martensitic phase transformations and magnetovolume effects in iron–nickel alloys are intimately related. The term Invar is widely used to characterize the unusual physical properties accompanying structural and magnetic instabilities such as those observed in the vicinity of the critical composition Fe₆₅Ni₃₅. We discuss the crossover from bulk iron–nickel alloys to nanoparticles with respect to structural and magnetic behavior. By employing molecular-dynamics and Monte Carlo methods, we find the absence of structural instabilities in defect-free particles, a linear scaling of the austenitic transformation temperature with the reciprocal cluster radius, as well as a decrease of the magnetic transition temperature with decreasing particle size.

Keywords: Martensitic and magnetic phase transitions; Iron–nickel nanoparticles; Molecular-dynamics; Monte Carlo simulations

1. INTRODUCTION

Martensitic instabilities, shape memory, and magnetovolume effects in iron-based alloys are of particular scientific and technological interest. In spite of the large amount of experimental data and numerous theoretical investigations there are basically unsolved problems – for a review and further discussion see Wassermann (1990). Although *ab initio* and model calculations have helped to understand basic features of the instabilities, further, in particular finite-temperature calculations of correlation functions are required to elucidate the interplay of electronic, magnetic, and lattice dynamics (for a recent discussion of dynamical aspects of phase transformation in solid iron using multimillion-atom molecular-dynamics simulations see Kadau *et al.* (2002); a recent review on the magnetochemical origin of Invar anomalies in iron–nickel alloys is given by Crisan *et al.* (2002). Figure 1 shows the instabilities of Fe–Ni bulk systems as a function of composition (Schröeter *et al.*, 1995; Entel *et al.*, 1998; Kadau, 2001; Crisan *et al.*, 2002). In this work we extend the investigations to iron–nickel nanoparticles by using molecular-dynamics and Monte Carlo methods.

*Corresponding author. Tel.: +49 203 379 3330. Fax: +49 203 379 3665. E-mail: entel@thp.uni-duisburg.de

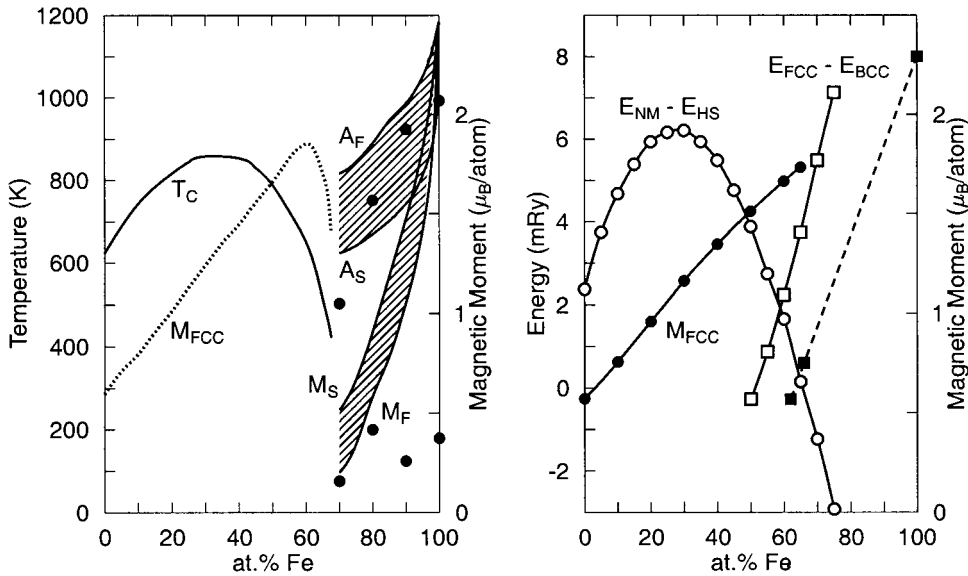


FIGURE 1 The experimental phase diagram (left panel) shows the variation of the Curie temperature T_C and the magnetization M_{FCC} with composition of the iron–nickel alloys with fcc structure. On the iron-rich side $A_{S,F}$ and $M_{S,F}$ denote the austenite and martensite start and final temperatures, respectively. The filled circles are results of molecular-dynamics simulations employing model potentials (upper dots: $\alpha \rightarrow \gamma$ transition with increasing temperatures; lower dots: $\gamma \rightarrow \alpha$ transition with decreasing temperatures (Entel *et al.*, 1998; Kadau, 2001). The “theoretical phase diagram” (right panel) shows the energy differences between the nonmagnetic (NM) and ferromagnetic (HS: high spin) ground states, $E_{NM} - E_{HS}$, of the alloys with fcc structure and the energy differences between the fcc and bcc structures on the iron-rich side: open squares mark single-site KKR CPA calculations by Schröter *et al.* (1995) and filled squares are results of multisite KKR CPA calculations by Crisan *et al.* (2002). The filled circles are the *ab initio* results for the magnetic moments.

Molecular-dynamics simulations were performed by using embedded-atom method (EAM) potentials specially designed to model the iron–nickel system (Meyer and Entel, 1998). We show that the austenitic transformation temperature of the iron–nickel particles depends on the particle size and scales with the inverse particle diameter d (see Fig. 2).

Of further interest is the consolidation process (sintering) of nanoparticles leading to nanocrystalline metals having interesting properties which differ from those of usual polycrystalline samples or single crystals (Liu *et al.*, 1994). Examples are the unusual low-frequency vibrational properties of nanocrystalline nickel or copper (Derlet *et al.*, 2001) and the increasing hardness with decreasing grain size due to dislocation immobilization at the grain boundaries known as Hall–Petch effect (Hall, 1951; Petch, 1953). Figure 3 shows the latter effect for a variety of nanophase metals (Siegel and Fougere, 1990). If, however, the average grain size is below a critical value, sliding in the grain boundaries due to the enormous amount of grain boundary atoms as compared to the atoms in the grains, becomes important. This leads to a softening at the smallest grain sizes which is called the reverse Hall–Petch effect (Chockshi *et al.*, 1989; Hahn *et al.*, 1997; Schiøtz *et al.*, 1998). All these effects obey scaling laws (e.g. hardness scales linear with the inverse square root of the grain sizes) similar to those that we observe in single nanoparticles.

Since the EAM model does not include magnetic degrees of freedom, we use, in order to treat magnetism of nanoparticles explicitly, an extended Ising model for coupled magnetic and spatial degrees of freedom, whereby the exchange integrals are taken from first-principles calculations. We show that for iron particles in the fcc structure the Néel temperature varies strongly with particle size. *Ab initio* calculations for smaller iron clusters show that the magnetic moments are not homogeneous over the cluster but increase considerably toward the surface of the cluster. This may explain the experimental observation that the average magnetic moment of the clusters increases with decreasing cluster size (Billas *et al.*, 1993, 1994, 1997; Apsel *et al.*, 1996) due to the increasing ratio of the number of atoms in the surface to the number of atoms in the volume. Recent first-principles calculations of iron clusters up to 62 atoms show that the magnetic moments of surface-layer atoms are much larger than bulk magnetic moment (Postnikov, 2002).

2. STRUCTURAL INSTABILITY OF IRON–NICKEL CLUSTERS

Figure 1 shows the details of the Fe–Ni phase diagram; experimental data have been taken from Wijn (1991) and Swartzendruber *et al.* (1993). One should point out the anomalously large hysteresis associated with the structural transformation for alloys on the Fe-rich side of the phase diagram and the break-down of magnetic order in the Invar region (Wassermann, 1990). In contrast to Fe–Ni alloys, the corresponding width of the structural hysteresis in nonmagnetic Hume–Rothery alloys is of the order of a few Kelvin (Ahlers, 1986). If one plots the variation of energy differences, obtained from zero-temperature *ab initio* calculations, with alloy composition experimental trends of transition temperatures are reproduced (Schröter *et al.*, 1995). Molecular-dynamics simulations relying on EAM potentials (Daw and Baskes, 1983, 1984; Daw *et al.*, 1993) show that the austenitic transformation (achieved with increasing temperature) is an entropy driven phase transition, whereas details of the martensitic transformation (obtained by decreasing the temperature from the high-temperature phase) depend crucially on the lattice defect which is responsible for initiating the nucleation process (Entel *et al.*, 1998; Kadau, 2001; Kadau *et al.*, 2001). In this contribution we examine the change of structural and magnetic instabilities of Fe–Ni clusters with respect to the corresponding bulk behavior. Of particular interest is the variation of the critical temperature with cluster size. The simulations are based on molecular-dynamics and Monte Carlo methods by using EAM model potentials and exchange constants fitted to experimental and *ab initio* data (Meyer and Entel, 1998; Entel *et al.*, 1998, 2000; Gruner *et al.*, 1998, 2000; Herper, 2000; Kadau, 2001; Kadau *et al.*, 2001, 2002).

Here we give a brief review of the results; for details we refer to the publications cited above and to unpublished work of Kadau (2001). The molecular-dynamics simulations show that structural changes occur on a time scale of picosecond although the dynamics of the dominant phonon-assisted shear deformation has so far not been resolved in the simulations. Orientational relationships between austenitic and martensitic structures are fairly well reproduced and agree with experiment (Entel *et al.*, 1998; Kadau, 2001). Furthermore we observe two new effects. First, the austenitic transformation temperature varies strongly with the cluster size and shows a linear scaling as function of the reverse cluster diameter. This can be explained by relating the transition

temperature to the difference in surface energies of the clusters with fcc and bcc structures, respectively,

$$\Delta E_S^{\text{fcc-bcc}}/\Delta E_B^{\text{fcc-bcc}} \propto 1/d, \quad (1)$$

where S stands for surface and B for bulk. Corresponding results for Fe–Ni clusters with different composition and size are shown in Fig. 2. Such a scaling behavior of critical temperatures for clusters with the inverse of the cluster diameter is not completely new. For instance, the melting temperature of clusters is predicted to scale as

$$1 - T_M(d)/T_B \propto 1/d, \quad (2)$$

which is based on a model known as “thermodynamic size effect” (Pavlow, 1909a,b) $T_M(d)$ and T_B are the melting temperatures for a cluster of diameter d and the corresponding bulk system, respectively (Buffat and Borel, 1976; David *et al.*, 1995; Lereah *et al.*, 2001). In the original work by Pavlow (1909a,b) a liquid or solid spherical particle with radius r , surface tension γ_S , vapor tension γ_V , density ρ of the solid or liquid, and specific volumes v was expressed as $c\gamma_V = \gamma_S/(RTrv\rho)$, where c is a constant, R the gas constant and T the temperature. Differentiating this equation and combining with the Clausius–Clapeyron equation yields a relation for the variation of melting temperature with the cluster size.

The scaling of T_M with $1/d$ seems not to be too much influenced by correlated orientations of nanocrystalline fluctuations, which are observed in experiments (Ben-David *et al.*, 1997) and also by molecular-dynamics simulations (Kreth, 2002) of melting of nanoparticles. Also surface-melting induced preroughening (Jaga *et al.*, 1999) does not change the scaling behavior. However, in larger nanoparticles above a few nanometers, when melting below T_M , a liquid layer much thicker than the corresponding

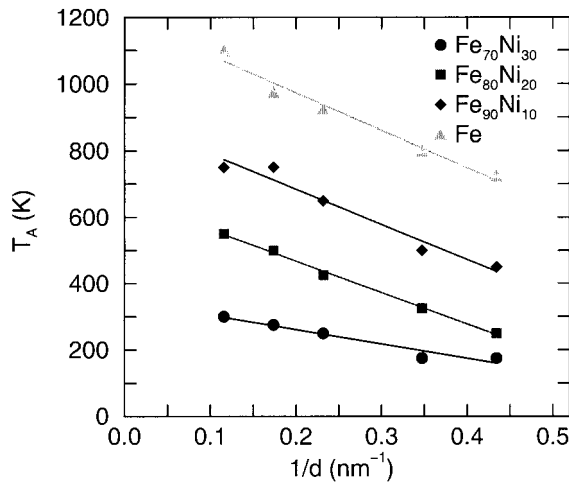


FIGURE 2 Variation of the austenitic transformation temperature T_A of Fe–Ni clusters as a function of the inverse cluster diameter d . The extrapolation of $d \rightarrow \infty$ yields transformation temperatures which lie within the range of experimentally observed austenitic start and final temperatures, see the phase diagram in Fig. 1.

layer on the bulk (with zero curvature) is formed (Kofman *et al.*, 1994). In this case the melting and freezing temperatures are different (Vanfleet and Mochel, 1995) and a nonlinear relationship between the melting point and the reciprocal of the radius can be expected (Sakai, 1996). For a recent review of melting and freezing we refer to Löwen (1994).

The scaling behavior defined in Eq. (2) has been confirmed by molecular-dynamics simulations of Al clusters with diameters up to $d = 5$ nm (Kreth, 2002). There is practically no departure from the $T_M \propto 1/d$ behavior. In the simulations we have used an EAM potential which was constructed with the help of experimental and *ab initio* data (Grabowski *et al.*, 2002). Corresponding simulations with Fe–Ni clusters yield too high melting temperatures, a short-coming of the used EAM potentials which are too repulsive upon compression (Kadau *et al.*, 2002). With respect to the freezing of clusters we expect a similar crucial dependence on size and on nucleation centers as in the case of martensitic transformations (Kadau, 2001; Kadau *et al.*, 2001).

Scaling behavior of different nature has been observed in nanocrystalline materials with respect to the change of plasticity, for a brief review see Schiøtz *et al.* (1998). In conventional metallic materials the hardness varies with the grain size through the empirical Hall–Petch relation (Hall, 1951; Petch, 1953; Nieh and Wadsworth, 1991) as

$$H_V = \sigma_y + k_y d^{-1/2}, \quad (3)$$

where H_V is the hardness, σ_y is the intrinsic stress resisting dislocation motion, d is the diameter of the grains and k_y is a constant. The effect is caused by the grain boundaries, impeding the generation and (or) motion of dislocations as the grains get smaller. This behavior extends into the nanocrystalline regime. For example, nanophase Fe hardens by a factor of 2.5 to 7 depending on how the nanophase material has been formed. A plot of the scaling behavior of experimental data, obeying the above law, can be found in Siegel and Fougere (1990) and is reproduced in Fig. 3.

But in very small nanoparticles the effect is often seen to cease or even to reverse because of increase of porosity, suppression of dislocation pile ups, diffusional creep in the grain boundaries and above all, because of sliding in the grain boundaries (Chockshi *et al.*, 1989; Hahn *et al.*, 1997; Schiøtz *et al.*, 1998). However, a satisfying theoretical description of the change of scaling behavior in Eq. (3), when going to ultrafine nanoparticles, is not at hand. We observe in all molecular-dynamics simulations of ultrafine Fe–Ni nanoparticles after sintering the reverse Hall–Petch effect.

3. MAGNETIC INSTABILITY OF IRON CLUSTERS

Besides structural transformations of Fe–Ni clusters magnetic phase transitions are of interest. From the corresponding bulk materials we know that both kind of instabilities occur simultaneously for the Fe–Ni alloys with compositions close to Invar, $\text{Fe}_{65}\text{Ni}_{35}$. In order to limit the discussion, we give a brief account of results for elemental fcc iron alone; for a discussion of Fe–Ni alloys we refer to Gruner *et al.* (1998).

In contrast to the Fe–Ni alloys with Invar behavior (reduced thermal expansion below the Curie temperature) fcc iron is known for its anti-Invar behavior, i.e., an enhanced thermal expansion at elevated temperatures. This effect is (like in Invar)

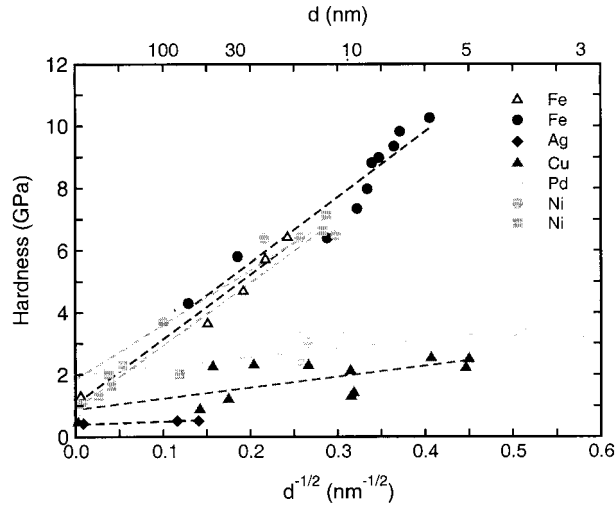


FIGURE 3 Variation of the hardness with $d^{-1/2}$, where d is the grain size, for a selected class of nanophase metals synthesized from gas-condensed clusters compared with their coarse-grained counterparts (values at $d^{-1/2} \rightarrow 0$). Values have been taken from Siegal and Fougere (1990) which also gives the references of the original works.

due to the strong mutual interaction of magnetic and elastic degrees of freedom. Fcc iron, however, is only stable at temperatures above 1183 K. The ground state properties of magnetism in fcc iron are well examined by means of Density Functional Theory (Herper *et al.*, 1999), showing that within the energy vs volume plane several magnetic solutions (ferromagnetic and antiferromagnetic) with different elastic properties exist, separated by only a few mRy in energy. It is possible to describe the relationship between the different magnetic solutions in terms of a localized spin model with distance dependent exchange interactions. For a given volume the interaction parameters $J_{ik}(r_{ik})$ are calculated, so that differences between *ab initio* $E(V)$ curves for the diverse magnetic structures (Herper *et al.*, 1999; Herper, 2000) are reproduced. The interaction parameters obtained by Herper (2000) are shown in Fig. 4. These data are used as input in the Monte Carlo simulations (Allen and Tildesley, 1987) of an effective spin model consisting of nearest and next-nearest neighbor exchange interactions and a simple Lennard–Jones pair-potential to account for magnetovolume effects. The corresponding Hamiltonian is given by

$$H = \sum_{(\text{NN}, \text{NNN})} J_{ik}(r_{ik}) S_i S_k + 4\varepsilon \sum_{(\text{NN})} \left\{ \left(\frac{r_{ik}}{\sigma} \right)^{12} - \left(\frac{r_{ik}}{\sigma} \right)^6 \right\}, \quad (4)$$

where the summations cover nearest (NN) and next-nearest (NNN) neighbors, respectively. The parameters $\varepsilon = 43.4$ mRy and $\sigma = 2.227$ Å of the Lennard–Jones model account for the basic elastic properties of fcc iron. Computational details are similar to previous works described in Gruner *et al.* (1998, 2000). The choice of an Ising model, thus neglecting spin-wave excitations, is a crude simplification but a straightforward extension of the *ab initio* calculations in which only collinear magnetic structures were considered (Herper *et al.*, 1999).

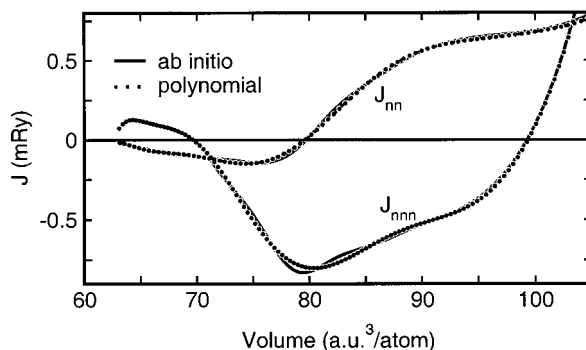


FIGURE 4 The nearest neighbor and next-nearest neighbor exchange parameters as obtained by *ab initio* calculations and the polynomial fit used in the simulations.

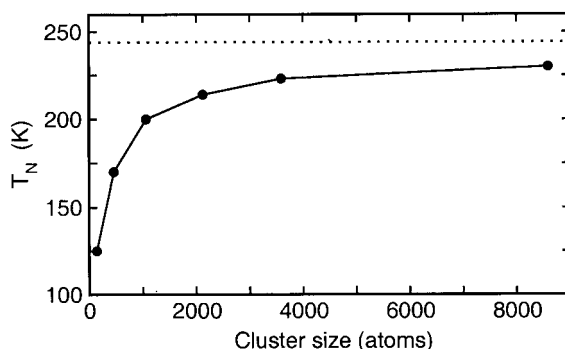


FIGURE 5 The Néel temperature of fcc Fe clusters as a function of the cluster size. Note that the Néel temperature scales approximately with the inverse of the cluster diameter.

In the bulk system the ground state is given by an antiferromagnetic structure of Type II, which is characterized by four interpenetrating perfectly antiferromagnetically ordered simple cubic sublattices. This structure is favored because of the strong antiferromagnetic exchange between next-nearest neighbors around the equilibrium volume. The antiferromagnetic order vanishes above the Néel temperature of $T_N = 244$ K. For small particles the transition temperature decreases sharply with decreasing cluster size, see Fig. 5. Clusters of 500 atoms and less do not show magnetic order above $T = 170$ K. However, a simple functional dependence between T_N and cluster size cannot be established on the basis of these data. The transition temperatures were determined by the inflexion points of the temperature dependence of the order parameter, which becomes increasingly smeared out with decreasing system size, see Fig. 6. Therefore, the values for T_N for small cluster have to be taken with some caution.

The thermal expansion behavior for various cluster sizes is shown in Fig. 7. Since the notion of the volume of the particle is subject to interpretation, we instead show the evolution of the mean nearest neighbor distance with temperature. As Fig. 7 shows, all clusters undergo a considerable contraction around the Néel temperature. This suggests that fcc iron, if it were stable around T_N , would show Invar behavior before

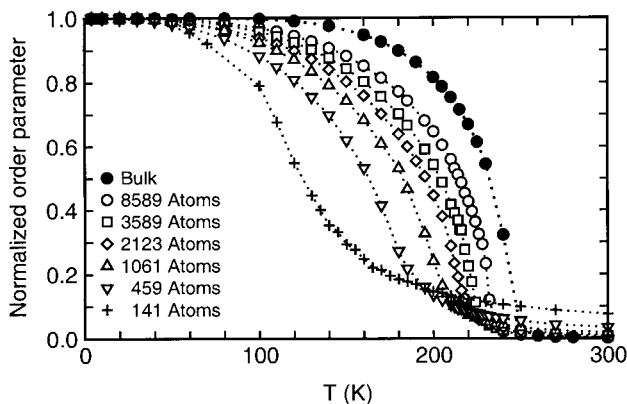


FIGURE 6 The antiferromagnetic order parameter as a function of temperature for various cluster sizes. Due to the low formation energy of antiferromagnetic domains, the original order parameter does not reach unity upon cooling down. Therefore, it had to be normalized to its low temperature value to allow for a comparison between the curves.

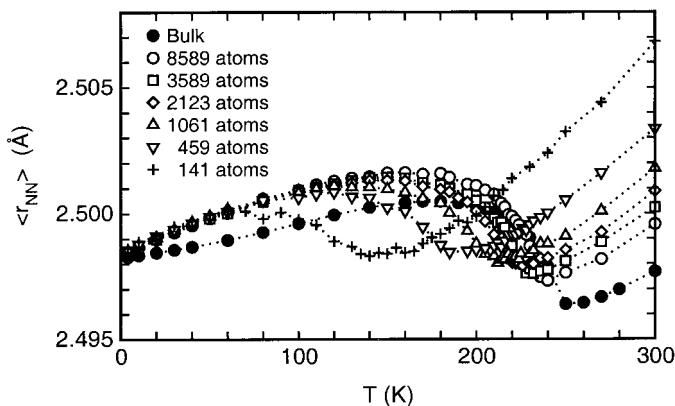


FIGURE 7 The averaged nearest neighbor distance vs temperature for various cluster sizes. Note the appearance of low thermal expansion around the Néel temperature.

becoming an anti-Invar material at higher temperatures. In this context we refer to particular Fe–Mn–Ni alloys which exhibit, for example, the Invar effect below the Curie temperature and the anti-Invar effect above it (Acet *et al.*, 1994); for elemental fcc Fe this kind of anomaly, where the Néel temperature would separate the low-temperature Invar from the high-temperature anti-Invar, has so far not been found experimentally. The contraction in Fig. 7 is shifted to lower temperatures with decreasing cluster sizes and becomes gradually flattened as the breakdown of the order parameter smears out due to finite size effects. Above T_N thermal expansion increases with decreasing cluster size, since the fraction of atoms on the surface with smaller coordination and thus weaker binding becomes larger.

The extrapolation of the Néel temperature to its bulk value yields a transition temperature of ≈ 240 K which is too large compared to the experimental value which is of the order of 67 K (Onodera *et al.*, 1994). We attribute this to the fact that an

Ising model has been used in the simulations. We expect that comparable simulations with a Heisenberg model will lower the Néel temperature considerably.

4. CONCLUDING REMARKS

In this brief review of structural and magnetic phase transitions in Fe–Ni nanoparticles we have addressed some new features like the scaling behavior of structural and magnetic transition temperatures with the inverse of the particle diameter. We could relate the scaling behavior to different surface effects in the two different phases. There are other properties of nanoparticles and agglomeration of nanoparticles with respect to which one is tempted to formulate a universal description. This includes, for example, the inverse Hall–Petch effect and the vibrational density of states of different kinds of metallic particles, see Derlet *et al.* (2001). Further scaling relations are known to exist with respect to the sintering of particles, which are based on phenomenological formulations for ideal situations like, for example, the time required for the coalescence of two perfectly spherical nanoparticles. The scaling of time for the sintering process in terms of the diameter of the particles has not been addressed in this contribution. The reason is that this type of scaling is usually not observed in the simulations because of the formation of crystalline surfaces with time of the initially spherical particles.

Acknowledgments

One of us (M.K.) acknowledges support by the German Science Council (Graduate College “*Structure and Dynamics of Heterogeneous Systems*”). This work has been supported by the Department of Energy (DOE).

References

- Acet, M., Zähres, H., Wassermann, E.F. and Pepperhoff, W. (1994). High temperature moment-volume instability and anti-invar of γ -Fe. *Phys. Rev. B*, **49**, 6012.
- Ahlers, M. (1986). Martensite and equilibrium phases in Cu-Zn and Cu-Zn-Al alloys. *Progr. Mater. Sci.*, **30**, 135.
- Allen, M.P. and Tildesley, D.J. (1987). *Computer Simulation of Liquids*. Clarendon, Oxford.
- Apsel, S.E., Emmert, J.W., Dens, J. and Bloomfield, L.A. (1996). Surface-enhanced magnetism in nickel clusters. *Phys. Rev. Lett.*, **76**, 1441.
- Ben-David, T., Lereah, Y., Deutscher, G., Penisson, J.M. *et al.* (1997). Correlated orientations in nanocrystalline fluctuations. *Phys. Rev. Lett.*, **78**, 2585.
- Billas, I.M.L., Becker, J.A., Châtelain, A. and de Heer, W.A. (1993). Magnetic moment of iron clusters with 25 to 700 atoms and their dependence on temperature. *Phys. Rev. Lett.*, **71**, 4067.
- Billas, I.M.L., Châtelain, A. and de Heer, W.A. (1994). Magnetism from the atom to the bulk in iron, cobalt, and nickel clusters. *Science*, **265**, 1682.
- Billas, I.M.L., Châtelain, A. and de Heer, W.A. (1997). Magnetism of Fe, Co and Ni clusters in molecular beams. *J. Magn. Magn. Mater.*, **168**, 64.
- Buffat, P. and Borel, J.-P. (1976). Size effect on the melting temperature of gold particles. *Phys. Rev. A*, **13**, 2287.
- Chockshi, A.H., Rosen, A., Karch, J. and Gleiter, H. (1989). On the validity of the Hall-Petch relationship in nanocrystalline materials. *Scripta Metall. Mater.*, **23**, 1679.
- Crisan, V., Entel, P., Ebert, H. and Akai H. *et al.* (2002). Magnetochemical origin for Invar anomalies in iron-nickel alloys. *Phys. Rev. B*, **66**, 014416.

- David, T.B., Lereah, L., Deutscher, G., Kofman, R. *et al.* (1995). Solid-liquid transition in ultra-fine lead particles. *Phil. Mag. B*, **71**, 1135.
- Daw, M.S. and Baskes, M.I. (1983). Semiempirical, quantum mechanical calculation of hydrogen embrittlement in metals. *Phys. Rev. Lett.*, **50**, 1285.
- Daw, M.S. and Baskes, M.I. (1984). Embedded-atom method: derivation and application to impurities, surfaces, and other defects in metals. *Phys. Rev. B*, **29**, 6443.
- Daw, M.S., Foiles, S.M. and Baskes, M.I. (1993). The embedded-atom method: a review of theory and applications. *Mater. Sci. Rep.*, **9**, 251.
- Derlet, P.M., Meyer, R., Lewis, L.J., Stuhr, U. *et al.* (2001). Low-frequency vibrational properties of nanocrystalline materials. *Phys. Rev. Lett.*, **87**, 205501.
- Entel, P., Kadau, K., Meyer, R., Crisan, V. *et al.* (2000). Molecular-dynamics simulations of martensitic transformations. In: Kramer, B. (Ed.), *Advances in Solid State Physics*, Vol. 40, pp. 156–166. Vieweg, Braunschweig.
- Entel, P., Meyer, R., Kadau, K., Herper, H.C. *et al.* (1998). Martensitic transformations: first-principles calculations combined with molecular-dynamics simulations. *Eur. Phys. J. B*, **5**, 379.
- Grabowski, S., Kadau, K. and Entel, P. (2002). Atomistic modeling of diffusion in aluminum. *Phase Transitions*, **75**, 265.
- Gruner, M., Sil, S. and Entel, P. (2000). Monte Carlo study of the magnetoelastic properties of Fe-Ni clusters. In: Entel, P. and Wolf, D.E. (Eds.), *Structure and Dynamics of Heterogeneous Systems*, pp. 156–166. World Scientific, Singapore.
- Gruner, M.E., Meyer, R. and Entel, P. (1998). Monte Carlo simulations of high-moment – low-moment transitions in Invar alloys. *Eur. Phys. J. B*, **2**, 107.
- Hahn, H., Mondal, P. and Padmanabhan, K.A. (1997). Plastic deformation of nanocrystalline materials. *NanoStruct. Mater.*, **9**, 603.
- Hall, E.O. (1951). The deformation and ageing of mild steel: III. Discussion of results. *Proc. Phys. Soc. (London) B*, **64**, 747.
- Herper, H. (2000). Ab-initio-Untersuchung magnetischer und struktureller Eigenschaften von 3d-übergangsmetallen und ihren Legierungen. Ph.D. thesis, Gerhard-Mercator-Universität Duisburg.
- Herper, H.C., Hoffmann, E. and Entel, P. (1999). Ab initio full-potential study of the structural and magnetic phase stability of iron. *Phys. Rev. B*, **60**, 3839.
- Jaga, E.A., Preshipino, S. and Tosatti, E. (1999). Surface-melting-induced pre-roughening. *Phys. Rev. Lett.*, **83**, 2753.
- Kadav, K. (2001). Molekulardynamik-Simulationen von strukturellen Phasenumwandlungen in Festkörpern, Nanopartikeln und ultradünnen Filmen. Ph.D. thesis, Gerhard-Mercator-Universität Duisburg.
- Kadav, K., Entel, P., Germann, T.C., Lomdahl, P.S. *et al.* (2001). Large-scale molecular-dynamics study of the nucleation process of martensite in Fe-Ni alloys. *J. Phys. IV France*, **11/Pr8**, 17.
- Kadav, K., Germann, T.C., Lomdahl, P.S. and Holian, B.L. (2002). Microscopic view of structural phase transitions induced by shock waves. *Science*, **296**, 1681.
- Kofman, R., Cheyssac, P., Aouaj, A., Lereah, Y. *et al.* (1994). Surface melting enhanced by curvature effects. *Surf. Sci.*, **303**, 231.
- Kreth, M. (2002). Solid-state and liquid-state reactions in bulk materials and nanoparticles: a molecular-dynamics study. Diploma thesis, Gerhard-Mercator-Universität Duisburg.
- Lereah, Y., Kofman, R., Penisson, J.M., Deutscher, G. *et al.* (2001). Time-resolved electron microscopy studies of the structure of nanoparticles and their melting. *Phil. Mag. B*, **81**, 1801.
- Liu, C.-L., Adams, J.B. and Siegel, R.W. (1994). Molecular dynamics simulations of consolidation process during fabrication of nanophase palladium. *NanoStruct. Mater.*, **4**, 265.
- Löwen, H. (1994). Melting, freezing and colloidal suspensions. *Phys. Rep.*, **237**, 249.
- Meyer, R. and Entel, P. (1998). Martensite-austenite transition and phonon dispersion curves of Fe_{1-x}Ni_x studied by molecular-dynamics simulations. *Phys. Rev. B*, **57**, 5140.
- Nieh, T.G. and Wadsworth, J. (1991). Hall-Petch relation in nanocrystalline solids. *Scripta Metall. Mater.*, **25**, 955.
- Onodera, A., Tsunoda, Y., Kunitomi, N., Pringle, O.A. *et al.* (1994). Neutron-diffraction study of γ -Fe at high pressure. *Phys. Rev. B*, **50**, 3532.
- Pavlov, P.N. (1909a). Relation between melting point and surface energy. *J. Russ. Phys. Chem.*, **40**, 1022.
- Pavlov, P.N. (1909b). Relation between melting point and surface energy. *Z. phys. Chem.*, **65**, 1, 545.
- Petch, N.J. (1953). The cleavage strength of polycrystals. *J. Iron Steel Inst.*, **174**, 25.
- Postnikov, A.V. (2002). Density functional simulation of small Fe nanoparticles. *Phys. Rev. B*, submitted.
- Sakai, H. (1996). Surface-induced melting of small particles. *Surf. Sci.*, **351**, 285.
- Schiotz, J., Tolla, F.D.D. and Jacobsen, K.W. (1998). Softening of nanocrystalline metals at very small grain sizes. *Nature*, **391**, 561.
- Schröter, M., Ebert, H., Akai, H., Entel, H. *et al.* (1995). First-principles investigations of atomic disorder effects on magnetic and structural instabilities in transition-metal alloys. *Phys. Rev. B*, **52**, 188.

- Siegel, R.W. and Fougere, G.E. (1990). Mechanical properties of nanophase materials. In: Hadjipanayis, G.C. and Siegel, R.W. (Eds.), *Nanophase Materials, Synthesis – Properties – Applications, Vol. 260 of NATO ASI Series E*, pp. 233. Kluwer, Dordrecht.
- Swartzendruber, L.J., Itkin, V.P. and Alcock, C.B. (1993). Fe-Ni (Iron-Nickel). In: Okamoto, H. (Ed.), *Phase Diagrams of Binary Alloys, Volume 9 of Monograph Series on Alloy Phase Diagrams*, pp. 257. ASM International, Materials Park, Ohio.
- Vanfleet, R.R. and Mochel, J.M. (1995). Thermodynamics of melting and freezing in small particles. *Surf. Sci.*, **341**, 40.
- Wassermann, E.F. (1990). Invar: moment-volume instabilities in transition metals and alloys. In: Buschow, K.H.J. and Wohlfahrt, E.P. (Eds.), *Ferromagnetic Materials*, Vol. 5, Chapter 3, p. 237. Elsevier, Amsterdam.
- Wijn, H.P.J. (1991). Alloys between 3d elements. In: Wijn, H.P.J. (Ed.), *Magnetic Properties of Metals – d-Elements, Alloys and Compounds*, Chapter 2, pp. 22. Data in Science and Technology. Springer, Berlin.